Journal of Alloys and Compounds 509 (2011) 7121–7129

Contents lists available at ScienceDirect

Journal of Alloys and Compounds

journal homepage: www.elsevier.com/locate/jallcom

A diffuse phase transition study on Ba^{2+} substituted $(Na_{0.5}Bi_{0.5})TiO_3$ ferroelectric ceramic

K. Sambasiva Rao*, B. Tilak, K.Ch. Varada Rajulu, A. Swathi, Haileeyesus Workineh

Centre for Piezoelectric Transducer Materials, Department of Physics, Andhra University, Vishakhapatnam 530003, India

ARTICLE INFO

Article history:
Received 3 March 2010
Received in revised form 25 March 2011
Accepted 2 April 2011
Available online 8 April 2011

Keywords:
X-ray diffraction
Relaxors
Impedance spectroscopy
Conductivity

ABSTRACT

Polycrystalline perovskite lead free material $(Na_{0.5}Bi_{0.5})_{0.91}Ba_{0.090}TiO_3$ was prepared by solid state reaction method. The crystal structure examined by X-ray powder diffraction indicates that the material was single phase with tetragonal structure. Dielectric studies exhibit a diffuse phase transition and characterized by a strong temperature and frequency dispersion of permittivity which relates cation disorder at A-site and exhibits relaxor behaviour. The dielectric relaxation has been modeled using the Vogel–Fulcher relationship, the calculated activation energy found to be $E_a = 0.021$ eV. Complex impedance analysis indicates the system undergoing a polydispersive non-Debye type relaxation. Also, used to characterize grain and grain-boundary resistivities of Ba substituted $(Na_{0.5}Bi_{0.5})TiO_3$ ceramic. The phenomenon was also interpreted by accounting for microstructural differences. The corresponding relaxation times were also used to confirm the interpretation of complex impedance spectra. Overlapping of grain boundary and electrode relaxation processes can be separated above about 4000 C. Electrical modulus spectroscopy studies have been performed. The conductivity parameters such as ion-hopping rate (ω_p) and the charge carrier concentration (K^1) have been calculated using Almond and West formalism.

1. Introduction

In recent times, lead-free piezoelectric materials, such as langasite single crystals, ferroelectric ceramics with perovskite structure, and Bi-layered structure oxides have received a considerable attention owing to their device applications. A large number of ferroelectric and antiferroelectrics were discovered experimentally; with perovskite-type structure with a general formula $A^{2+}[B^1_xB^{11}_{1-x}]O_3$. In these compounds the A-ions (Na^+, K^+ and Bi^{3+}) are located at lattice sites with a coordination number 12, while, B-ions occupy with transition metal ions with inert gas electron structure (s^2p^6) in their ground state, e.g. Ti^{4+}, Zr^{4+}, Nb^{5+}, Ta^{5+}, etc. in octahedral positions [1].

Perovskite type sodium bismuth titanate ($Bi_{0.5}Na_{0.5}TiO_3$, NBT) was first reported by Smolenskii et al. [1]. NBT lead free relaxor ferroelectric material with excellent piezoelectric properties, can be effectively enhanced at morphotropic phase boundary (MPB) of the composition. It has rhombohedral symmetry at room temperature, it undergoes a series of phase transitions: (i) ferroelectric rhombohedral to antiferroelectric tetragonal around 230 °C, (ii) antiferroelectric tetragonal to non-polar tetragonal around 320 °C with broad maximum of electric permittivity, which may originate from dielectric relaxation due to the response of electromechanical interactions between polar regions and non-polar matrix [2], (iii) cubic to tetragonal symmetry takes place in the temperature range of 520–540 °C [3], where it is superparaelectric [4,5]. Further, NBT has relatively high Curie temperature (320 °C), relatively large remanent polarization ($p_r = 38\ \mu C/cm^2$) and coercive field ($E_c = 73$ kV/cm) at room temperature [1]. It is hard to be pole for its high coercive field and its high conductivity. To solve these problems and improve electrical properties, various types of compounds were added into NBT to form solid solutions such as $CaTiO_3$, $NaNbO_3$, $BaTiO_3$, etc. [6].

Among the NBT based system $(1-x)Bi_{0.5}Na_{0.5}TiO_3$-$xBaTiO_3$ possesses rhombohedral (FR)–tetragonal (FT) MPB boundary at $x = 0.06$–0.07 [7]. Gao et al. reported the composition $(1-x)BaTiO_3$-$xBi_{0.5}Na_{0.5}TiO_3$ with $x \geq 0.3$ mol start to exhibit the relaxor ferroelectric properties [8]. The polycrystalline NBT–6%BT system has been reported to exhibit piezoelectric constant, $d_{33} = 125$ pC/N and $k_{33} = 0.55$ near the rhombohedral/tetragonal MPB region [7]. These materials have indeed high electromechanical characteristics which can be controlled either by doping or by compositional change.

Transport and relaxation properties can be described at higher temperatures with reference to interparticle interaction. Impedance spectroscopy has been recognized as a powerful technique to distinguish the grain and grain boundary conductivity contribution of many oxide ceramics [9–11]. Traditionally, DC and

* Corresponding author.
E-mail address: Konapala@sify.com (K.S. Rao).

0925-8388/$ – see front matter © 2011 Elsevier B.V. All rights reserved.
doi:10.1016/j.jallcom.2011.04.021

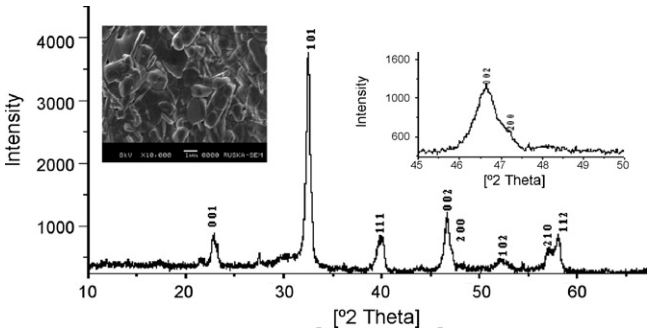

Fig. 1. XRD pattern for BNBT90.

fixed frequency AC measurements have been the preferred methods to characterize electro ceramics but these provide little or no information on electrical microstructure. Bauerle [10] was the first to show that AC methods could be used to separate the various resistances (R) and capacitance (C) values associated with the electrode reaction, grain boundary regions and grain interiors in ceramic solid electrolytes. From this study, it became apparent that AC techniques, particularly in the range 10^{-2}–10^{7} Hz, now commonly referred to as impedance spectroscopy (IS) could provide a method to probe the electrical microstructure of ceramics. The electrical conductivity studies indicate the nature of dominant constituents or charge species involved in the conduction on the application of an electric field.

In view of the important properties exhibited by the material and also conductivity, impedance spectroscopy studies have not been reported in the literature survey, an attempt has been made to study the structural, electrical properties of $(Na_{0.5}Bi_{0.5})_{0.91}Ba_{0.090}TiO_3$ ceramics. The permittivity (ε^*), impedance (Z^*), electrical modulus (M^*), and conductivity (σ^*) spectroscopy techniques have been studied over the wide range of temperature (35–600 °C) and frequency region (45 Hz to 5 MHz).

2. Experimental

Polycrystalline $(Na_{0.5}Bi_{0.5})_{0.91}Ba_{0.090}TiO_3$ (abbreviated as BNBT90) ceramic has been synthesized by high temperature solid state reaction technique. Initially, analar grade Na_2CO_3, Bi_2O_3, $BaCO_3$, and TiO_2, were mixed in stoichiometric ratio and grounded in agate mortar and pestle in methanol and calcined at 800 °C for 2 h. After confirming the formation of single phase composition by X-ray diffraction, adequate amount of polyvinyl alcohol was added and grounded well. Then the powder is pressed into pellet of 11 mm diameter and 2.5 mm thickness using an uniaxial pressure of 7 MPa in a stainless steel die. The pressed pellets were sintered at 1150 °C for 2 h in an air atmosphere. Silver electrodes were deposited on the polished surfaces of pellet to perform experimental studies.

The crystal structure of the material has been analyzed by X-ray diffractometer (Philips with CuKα radiation (λ = 1.5406Å)). The lattice parameters were estimated using Computer Program package-interpretation and Indexing program by E. Wu. School of Physical Science, Flinders University of South Australia. The microstructure on the specimens of present investigation was obtained with scanning electron microscope (SEM) (JEOL.JY: Model 5800F). The measurement of permittivity (ε^*), impedance (Z^*), electrical modulus (M^*), and conductivity (σ^*) as function of temperature (35–600 °C) and frequency (45 Hz to 5 MHz) have been carried out using computer interfaced LCR Hi-Tester (HIOKI 3532-50, Japan).

3. Results and discussion

3.1. Phase analysis

Fig. 1 shows the X-ray diffractogram of BNBT90 in the 2θ range 10–60°. All the peaks were indexed. XRD analysis on the material reveals it is a single phase with tetragonal structure.

Whereas XRD patterns with high Ba^{2+} concentration show strong (2 0 0) peak splitting which is indicative of the tetragonal phase and at low concentration of Ba^{2+} they show (2 0 0) peak transformed to a single peak which suggests rhombohedral symmetry, i.e., observed above and below of MPB region, respectively. The reflection at 47°, which is assigned as (0 0 2), (2 0 0) is confirmed to be a tetragonal phase [12]. The bulk density of sintered material has been measured by the Archimedes method; the experimental density achieved is 98% to that of theoretical density. The values of lattice parameters, density, and porosity of the material have been given in Table 1. The insert of Fig. 1 shows the SEM micrograph of polished surfaces of the sintered pellet of BNBT90. The grain size of the sample has been calculated from linear intercept method. The observed average grain size from micrograph is 0.97 μm.

Table 1
Lattice parameters.

Lattice parameters (Å)	Cell volume (Å^3)	Density (g/cm^3)		% density	Porosity
		ρ_{exp}	ρ_{cal}		
$a = b = 3.76$ $c = 3.89$	58.28	6.30	6.42	98	0.02

Table 2
Crystallite size.

Average crystallite size (nm)		Average micro strain ε ($\times 10^{-3}$)
Debye–Scherer technique	Williamson–Hall technique	
31	52	6.10

The average crystallite size of BNBT90 has been estimated from reflections of 2θ values of XRD profile using Debye–Scherer equation,

$$t = \frac{K\lambda}{B\cos\theta} \quad (1)$$

where t is the averaged dimension of crystallite, the Scherer constant ($K = 0.89$), λ is the wavelength of X-ray (λ = 1.5406 Å) and B = FWHM (full width half maxima) of broadening diffraction line on the 2θ scale (radian). The average crystallite size has been calculated by using the above formula and is given in Table 2.

Fig. 2 shows the Williamson–Hall plot approach [13]. The slope of the plot $B\cos\theta/\lambda$ versus $4\sin(\theta)/\lambda$ (Fig. 2) gives the value of microstrain and intercept results crystallite size. The values of average crystallite size and micro strain of the BNBT90 ceramic have been tabulated in Table 2.

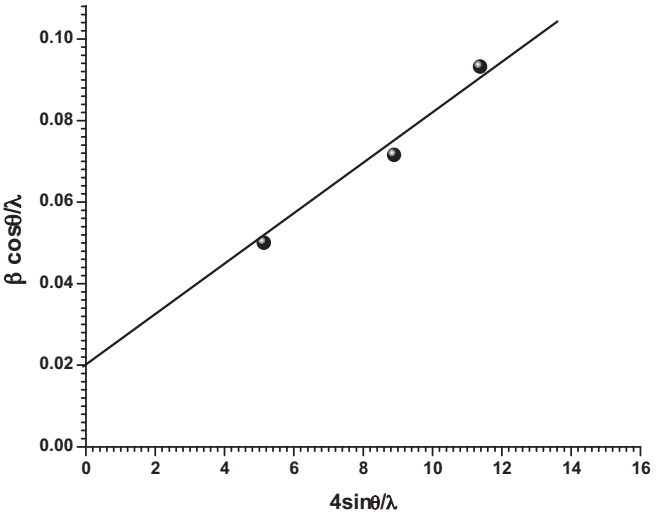

Fig. 2. Williamson–Hall plot.

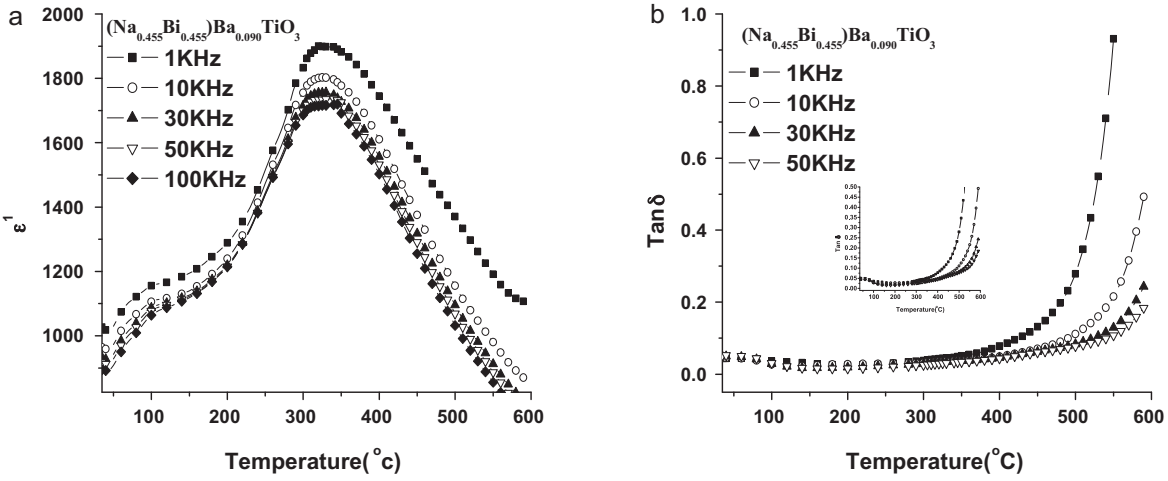

Fig. 3. Temperature dependence of (a) dielectric constant (ε^1) and (b) tan δ loss at different frequencies.

In Williamson–Hall method, the broadening due to strain is completely removed and so the crystalline size is larger, when compared to Debye–Scherer method. In BNBT90 system A-site is occupied by Na^{1+} = 0.97 Å, Bi^{3+} = 0.96 Å, Ba^{2+} = 1.34 Å, and Ti^{4+} = 0.68 Å ion occupied by the B-site of the perovskite. A simple description of the geometric packing within perovskite structure can be characterized by tolerance factor t, which is defined by following equation [14],

$$t = \frac{(r_A + r_o)}{\sqrt{2}(r_B + r_o)} \quad (2)$$

where r_A, r_B and r_o are ionic radii of A-site cation, B-site cation and anion, respectively. The value of t = 0.81 has been estimated and it is with in the limit of stable perovskite structure.

3.2. Dielectric studies

The temperature dependence of the dielectric constant (ε^1) and dielectric loss tangent (tan δ) in the 1–100 kHz frequency range is depicted in Fig. 3a and b. The dielectric response plot exhibited a diffuse phase transition (DPT) and the temperature of the dielectric maximum (T_m) shifts towards higher temperature side with increase in frequency which confirms the relaxor behaviour of the BNBT90 material. The 'tan δ' exhibited a frequency dependent phenomenon (Fig. 3b). At lower frequencies this anomaly in the loss curve is not much evident as the sample shows higher values of losses and perhaps due to the presence of the other relaxations particularly at higher temperatures.

The diffuse phase transition of BNBT90 can be described by the modified Curie–Wiess law,

$$\varepsilon^{-1} - \varepsilon_m^{-1} = A(T - T_m)^{\gamma} \quad (3)$$

where A is a constant and γ is the diffusivity parameter [15,16]. For normal ferroelectrics γ is less than 1 and it is 1–2 for relaxor ferroelectric. Fig. 4 shows the variation of $\ln(\varepsilon_m/\varepsilon_r - 1)$ with $\ln(T - T_m)$ for BNBT90 at 1 kHz. To estimate the value of γ, the experimental data has been fitted to Eq. (3).

The plot shows a linear behaviour with temperature and the value of γ computed to be 1.83, which clearly indicates the DPT behaviour. It is expected that some disorder in the cation distribution (compositional fluctuations) causes the DPT where the local Curie points of different microregions statistically distribute around the mean Curie temperature [17].

Fig. 5 shows the variation of inverse of temperature T_m with $\ln(\nu)$ Hz. It can be observed from the figure that the frequency

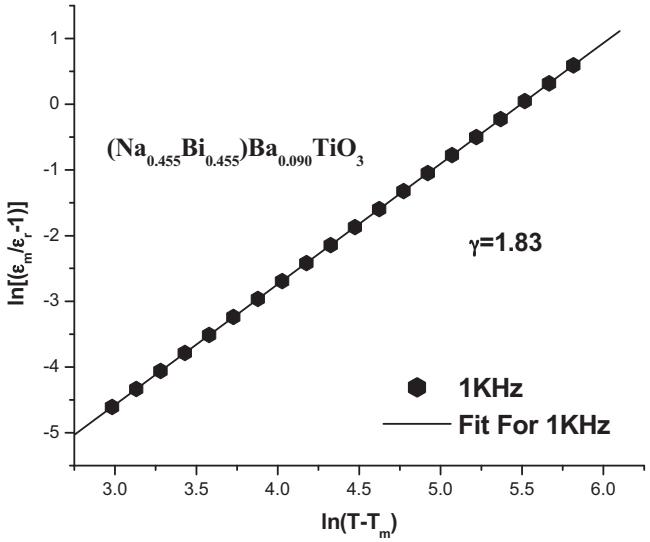

Fig. 4. Dependence of $\ln(\varepsilon_m/\varepsilon_r - 1)$ on $\ln(T - T_m)$ for BNBT90 at 1 kHz.

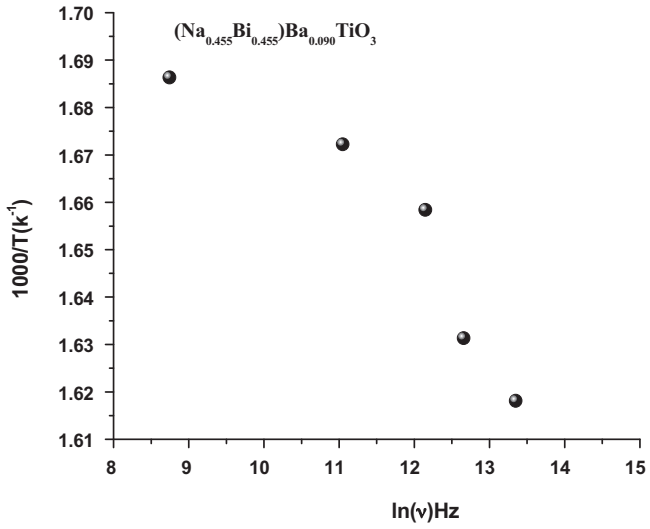

Fig. 5. Variation of Vogel–Fulcher relationship for BNBT90.

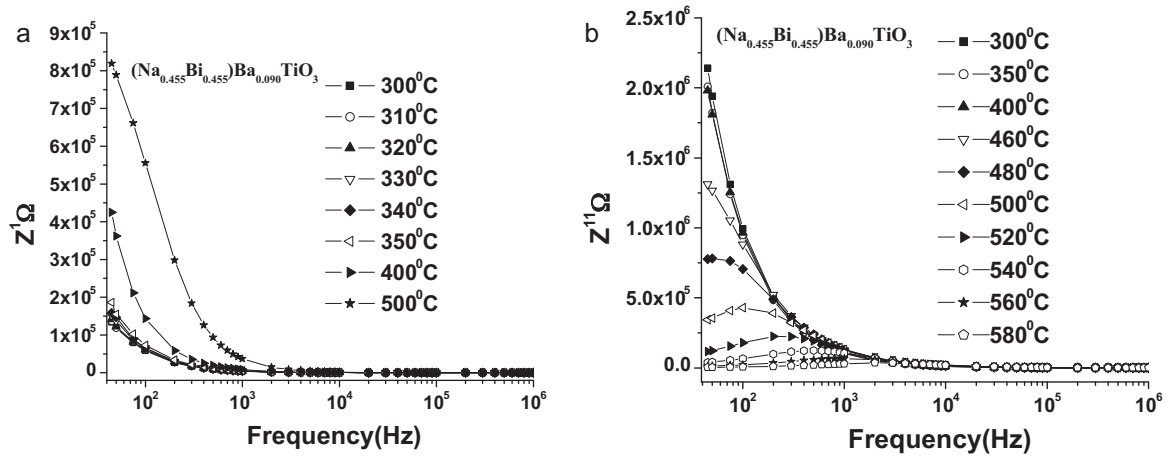

Fig. 6. Frequency dependence of (a) real part of impedance, (b) imaginary part of impedance.

derivative of $1/T_m$ is smaller at lower frequencies. This indicates as $f \rightarrow 0$, a static freezing temperature (T_f) is approached. The frequency dependence of the temperature of the permittivity maximum T_m has been modeled using the Vogel–Fulcher empirical relationship [18,19].

$$\nu = \nu_o \exp\left[\frac{-E_a}{k_B(T_m - T_f)}\right] \quad (4)$$

where ν, ν_o, k_B and E_a are, respectively the operating frequency, pre-exponential factor, Boltzmann constant and the activation energy. T_f is the freezing frequency. T_f is regarded as the temperature where the dynamic reorientation of the dipolar cluster polarization can no longer be thermally activated. An excellent fitting of Vogel–Fulcher relation with experimental data successfully explains the relaxor behaviour in BNBT90 ceramic. The values of E_a, ν_o, and T_f are found to be 0.021 eV, 2.2×10^6 Hz, 305 °C.

3.3. Impedance and modulus spectroscopy studies

The modulus plots give emphasis on elements of the ceramics with smaller capacitance, while impedance plots highlight the elements with largest resistance. Fig. 6a represents the real part of impedance (Z^1) as a function of frequency. Z^1 has higher values at lower frequencies and decreases up to 10 kHz and attains a constant value beyond. At lowest frequency, BNBT90 exhibited the value of $Z^1 = 158.940\,k\Omega$ (300 °C) and is increases to 822.893 kΩ (500 °C). The increase in impedance shows the decrease in conductivity as discussed above. The Z^{11} curves are also decreasing with increase of temperature. Further, irrespective of temperature, all the curves in both Z^1 and Z^{11} plots are found to be merging above 10 kHz, which is ascribed to release of space charge effect. The asymmetric broadening of Z^{11} peaks (Fig. 6b) suggests that there is a spread of relaxation times, i.e., the existence of a temperature dependent electrical relaxation phenomenon in the material [20]. At higher values of Z^1 and Z^{11} at lower frequencies and temperatures indicating a higher effect of polarization.

The normalized imaginary part, Z^{11}/Z^{11}_{max} of the impedance as a function of frequency at several temperatures in BNBT90 has been shown in Fig. 7a. It seems that high temperature (≥400 °C) triggers another (grain boundary) relaxation process. From the Arrhenius plot (Fig. 7b) the activation energy has been evaluated and found to be 0.85 eV.

Fig. 8 shows the complex impedance plots at different temperatures. It is observed that one semicircle is obtained from lower temperature and two semicircles could be obtained at higher temperature with different resistance for grain (R_b) and grain boundary (R_{gb}). Hence grain and grain boundary effects could be separated at these temperatures. It can also be observed that the peak maxima of the plots decrease and the frequency for the maximum shifts to higher values with the increase in temperature. The dielectric relaxation in the system can be assessed through complex impedance plots. The centers of the semicircles are laying below the real-axis,

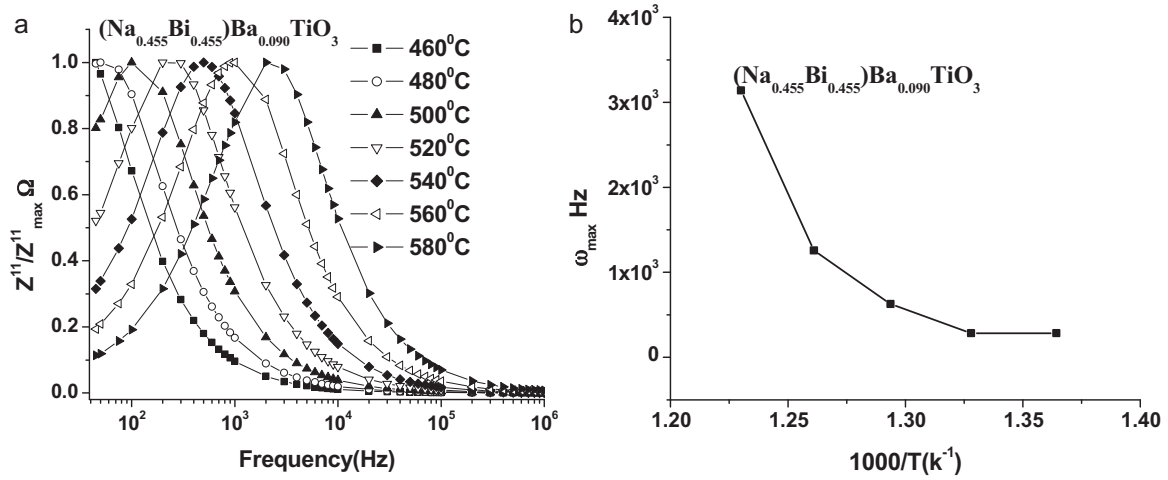

Fig. 7. (a) Normalized peak Z^{11}/Z^{11}_{max} at different temperatures, (b) Arrhenius plot of Z^{11} peak frequencies.

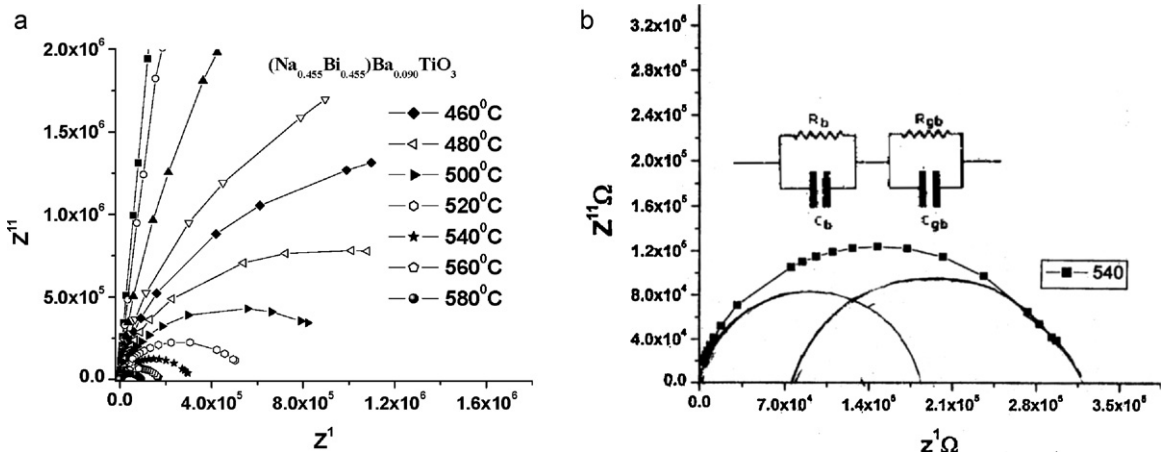

Fig. 8. Cole–Cole plots for BNBT90 at different temperatures, (b) equivalent circuit.

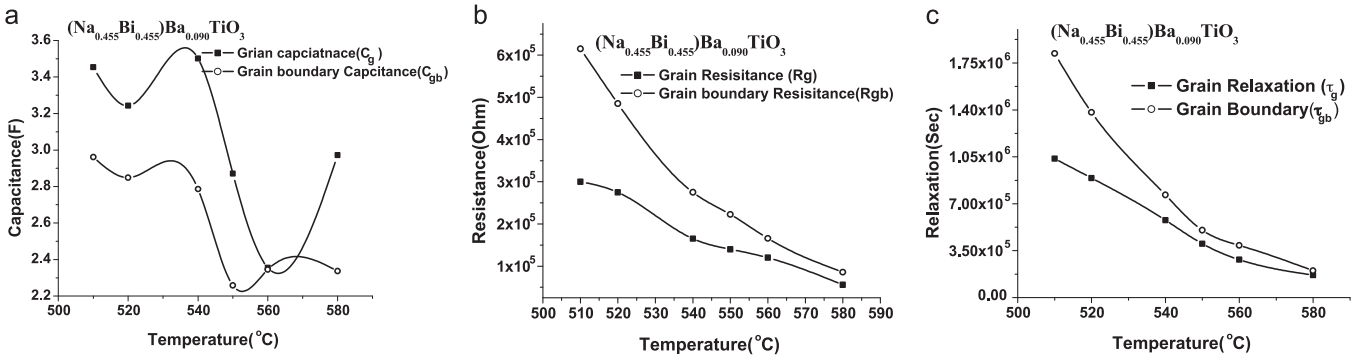

Fig. 9. Variation of capacitance, resistance and relaxation of grain, grain boundary with temperature on BNBT90.

revealing the non-Debye type relaxation in BNBT90. The complex impedance in such situations can be described as

$$Z*(\omega) = Z^1 + iZ^{11} = \frac{R}{1+(i\omega/\omega_o)^{1-\alpha}} \quad (5)$$

where α represents the magnitude of the departure of the electrical response from an ideal condition and this can be determined from the location of the center of the semicircles, when $\alpha \to 0$, Eq. (5) gives rise to classical Debye's formalism. It can be seen that the complex impedance plots are not represented by a full semicircle, rather center that the semicircle arc lies below the Z^1 axis ($\alpha > 0$) suggesting the dielectric relaxation to be of a non-Debye type. This may be due to the presence of distributed elements in the material-electrode system [21]. Since the relaxation times of the relaxator materials within polar clusters are distributed over a wide spectrum at higher temperatures, their response to external fields is in a different time domain. This results in the deviation from Cole–Cole plots. As the measuring temperature increases Cole–Cole plots split into two discrete semicircles, inferring the possible average profile of various Cole–Cole semicircles. The split semicircles may be due to secondary element like interfacial capacitance or defects. The first semicircle (may be ascribed to a parallel combination of bulk resistance, R_b and Capacitance C_b) in the high frequency region, corresponds to the behaviour of intragranular of the material or bulk properties. The second semicircle (may be attributed to parallel combination of grain boundary resistance, R_{gb} and capacitance C_{gb}), in the low frequencies region, and represents the grain boundary contribution. It is known that the conductivities of grains and grain boundaries may be different owing to the different underlying processes, and thereby they relax in different frequency regions.

Impedance can be represented as

$$Z* = (R_b^{-1} + j\omega C_b)^{-1} + (R_{gb}^{-1} + j\omega C_{gb})^{-1} \quad (6)$$

where

$$Z^1 = \frac{R_b}{1+(\omega R_b C_b)^2} + \frac{R_{gb}}{1+(\omega R_{gb} C_{gb})^2}$$

and

$$Z^{11} = \frac{\omega R_b^2 C_b}{1+(\omega R_b C_b)^2} + \frac{\omega R_{gb}^2 C_{gb}}{1+(\omega R_{gb} C_{gb})^2} \quad (7)$$

The values of R_g and R_{gb} could directly be obtained from the intercept of the ends of the semicircle on the Z^1-axis whose variation with temperature is shown in Fig. 8b. The temperature variation of C_g, C_{gb} and R_g and R_{gb} is shown in Fig. 9a and b. It observed that the values of R_g and R_{gb} decrease with rise of temperature. The capacitance (C_g and C_{gb}) is estimated using the relation.

$$\omega_{max}\,RC = 1 \quad (8)$$

Table 3
Activation energy values (eV) of conduction (E) and relaxation (e) for grain (g) and grain boundary (gb) of BNBT90.

Temperature range (°C)	Grain conduction activation energy, E_g (eV)	Grain boundary conduction activation energy, E_{gb} (eV)	Grain relaxation activation energy, e_g (eV)	Grain boundary relaxation activation energy, e_{gb} (eV)
500–580	0.47	0.71	0.88	0.83

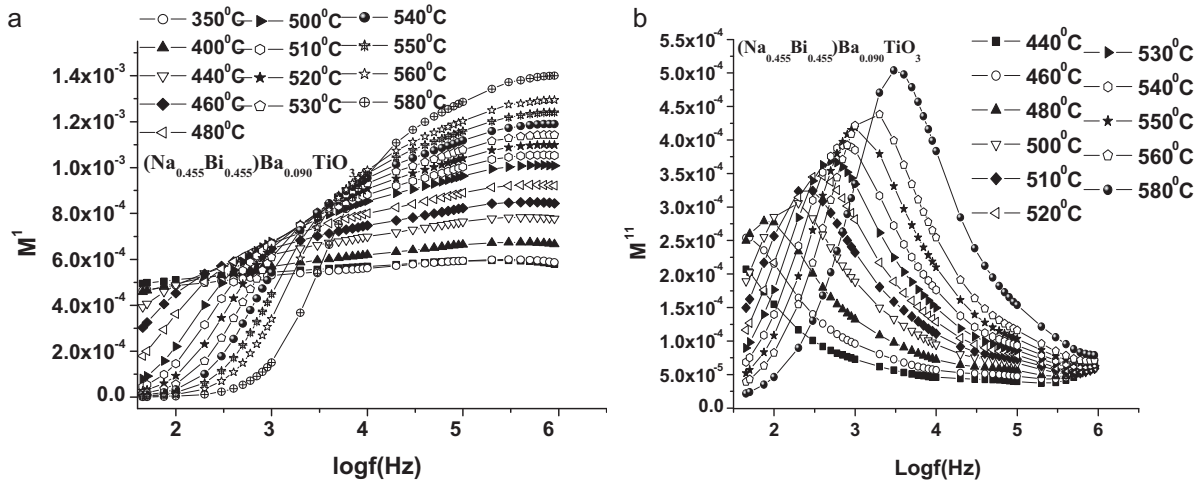

Fig. 10. (a) Variation of real part of modulus, (b) imaginary part of modulus as a function of frequency for BNBT90.

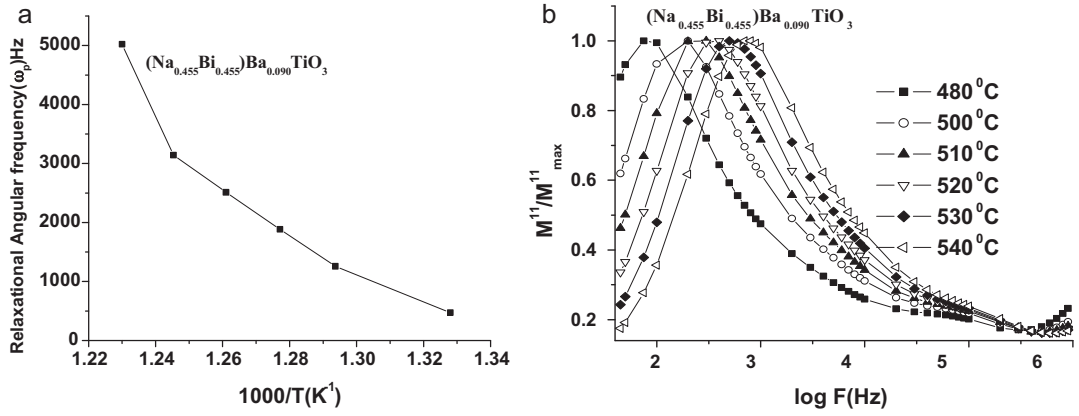

Fig. 11. (a) Variation of DC-conductivity relaxation time versus $1/T$ and (b) M^{11}/M^{11}_{max} as function of frequency for BNBT90.

where ω_{max} ($=2\pi f_{max}$) is the angular frequency at the maximum of the semicircle. The C_g and C_{gb} are obtained from Cole–Cole plots at different temperatures. The decrease in the value of R_g of BNBT90 is associated with an increase in conductivity with the rise in temperature. Also, a decrease in R_{gb} values with the increment in temperature suggests the lowering of the barrier to the mobility of charge carriers aiding electrical conduction at higher temperatures [22]. From Fig. 9c, it is observed that τ_g (grain relaxation) and τ_{gb} (grain boundary relaxation) decrease relaxation time with increase in temperature. The values of R_g, R_{gb}, τ_g, τ_{gb} show an Arrhenius behaviour. The grain and grain boundary conduction and relaxation activation energies are tabulated in Table 3. It is evident from the table that, the conduction mechanism is basically dominated by grain boundary conduction through hopping electrons created through oxygen vacancies.

3.3.1. Electrical modulus

Fig. 10a shows the variation of (a) real part of modulus, (b) imaginary part of modulus as function of frequency. M^1 increases with increase in frequency and almost takes a constant value beyond 10 kHz. At low frequency and high temperature region, M^1 approaches zero confirming an appreciable electrode and/or ionic polarization [23]. It is evident from Fig. 10b that there is a shift in the peak frequencies of M^{11} to higher frequency side as temperature increases. Increasing temperature, the DC conduction is attributed to long range motion of ions that are thermally activated.

The low frequency side of the peak represents the range of frequency in which the ions can move long range, i.e., ions can perform successfully hopping from one site to the neighboring site. The high frequency side of the M^{11} represents the range of frequencies in which the ions are separately confirmed their potential wells, and the ion can make only the localized motion within the well [24–27]. Also, M^{11} peak frequencies increase with increase in temperature and the shift in frequency of M^{11} peaks corresponds to the so-called conductivity relaxation. The activation energy of DC conduction 0.68 eV is obtained from Arrhenius plots (Fig. 11) of M^{11} peak frequency. The reciprocal of frequency of the M^{11} peak represents the time scale of the transition from long range mobility and is identified as the characteristics relaxation time. Fig. 11b shows the normalized imaginary part of the electrical modulus M^{11}/M^{11}_{max} as a function of frequency at several temperatures in BNBT90.

The M^{11}/M^{11}_{max} parameter exhibits a peak or maximum value with slightly asymmetric degree at each temperature. The region to the left and right side of this peak indicates the mobile carriers over long distance and confined to potential well, i.e., over a short distance, respectively. The frequency range at and around the peak indicates the transition from short to long range mobility, considering the decrease in frequency [28].

3.4. Electrical conductivity studies

Fig. 12 shows the variation of the AC conductivity as a function of frequency at some elevated temperatures in BNBT90.

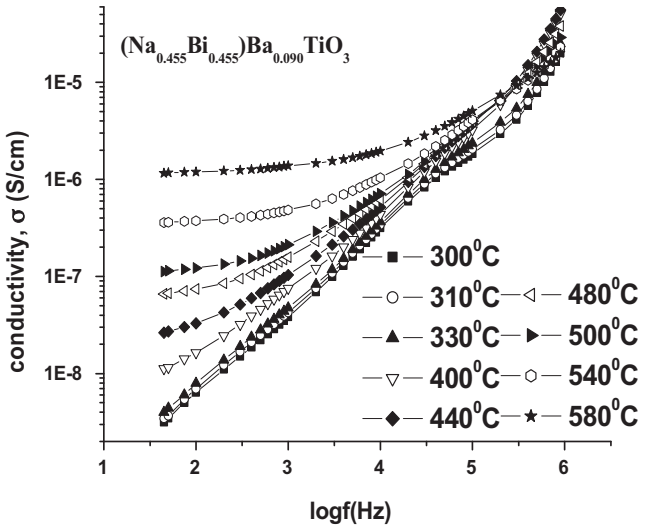

Fig. 12. Variation of AC conductivity as a function of frequency at different temperatures.

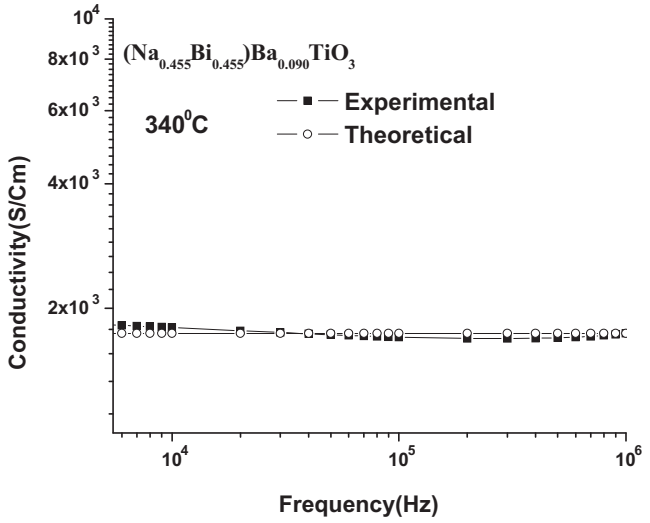

Fig. 14. Experimental and theoretical fit for AC conductivity as a function of frequency at 340 °C.

From Fig. 12, the occurrence of plateau like region in low frequency, at high temperature region reveals the frequency independent conductivity, i.e., DC like [σ_o]. The conductivity subsequently increases with increase of frequency, which varies approximately as a power of frequency (ω^n) (where n is a function of temperature as well as frequency) at all temperatures. The characteristic frequency which is the onset of ω^n dependence shifts towards higher frequency side with increase in temperature which attributes to the relaxor behaviour of the material. The conductivity spectra obey Jonscher's law and AC conductivity is found to vary with angular frequency,

$$\sigma = \sigma_o + A\omega^n \tag{9}$$

where σ_o is the DC conductivity, A and n ($0 < n < 1$) are the temperature dependent parameters. This power law is a universal property of materials and is related to the dynamics of hopping conduction.

The values of σ_o and A(T) have been determined by fitting frequency dependent conductivity data from Eq. (9). As shown in Figs. 13a and b and 14, ion hopping rates (ω_p) have been calculated using the formula proposed by Almond and West [29],

$$\omega_p = \left(\frac{\sigma_o}{A}\right)^{1/n} \tag{10}$$

The ion hopping rates, ω_p are following the Arrhenius relation and is thermally activated process,

$$\omega_p = \omega_e \exp\left(\frac{-H_m}{KT}\right) \tag{11}$$

where ω_e is the effective attempt frequency, H_m is the activation enthalpy for hopping or migration of ions. From Fig. 15, the value of H_m is found to be 0.24 eV.

The magnitude of the carrier concentration term K^1 has been determine by the relation [30],

$$K^1 = \frac{\sigma_T}{\omega_p} \tag{12}$$

Fig. 16 shows the temperature dependence of the charge carrier concentration (K^1). The charge carrier concentration is observed to be increasing with raise in temperature under investigation. This reveals the generation of charge carriers with increase of temperature and an active participation of oxygen vacancy conduction in BNBT90. Therefore, the activation energy calculated from the Arrhenius plot of conductivity represents the energy required for the migration of ions.

Fig. 17 shows, Arrhenius AC conductivity plot with inverse of temperature at different frequencies. At low temperatures up to at about 200 °C, the conductivity does not show any appreciable change for all the frequencies of measurement. At 1 kHz, the

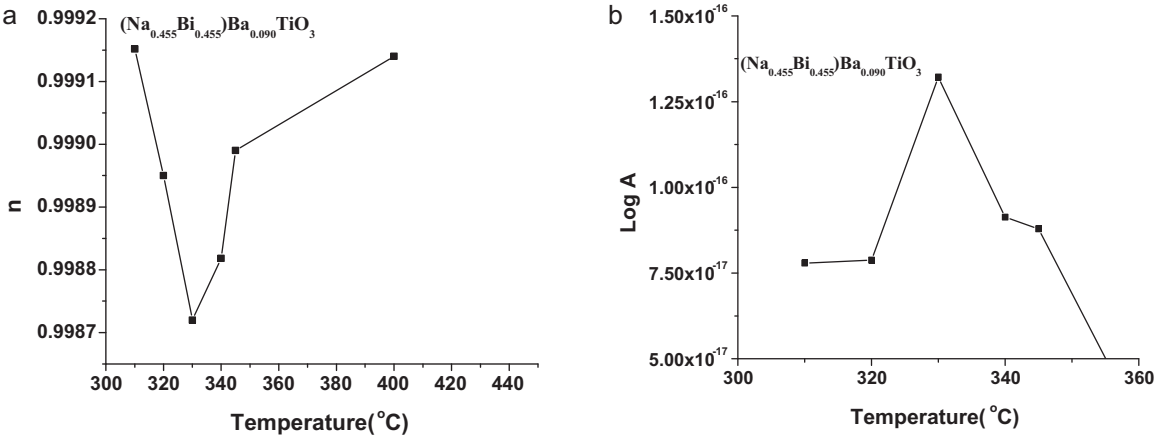

Fig. 13. (a) Variation of (a) n as function temperature, (b) A as a function of temperature.

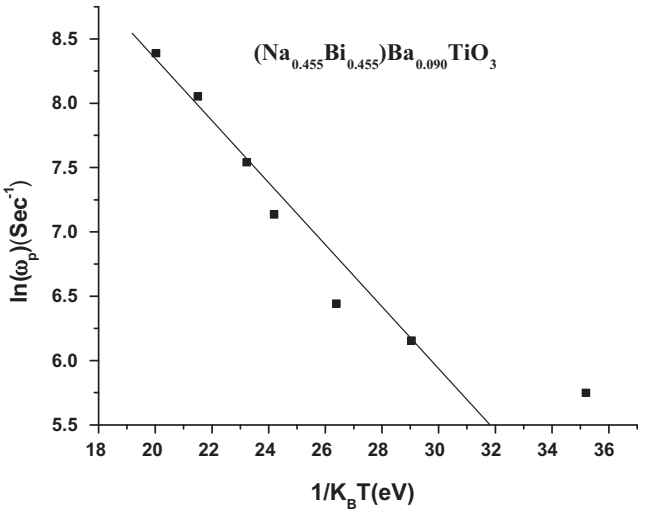

Fig. 15. The temperature dependence of hopping rate for BNBT90.

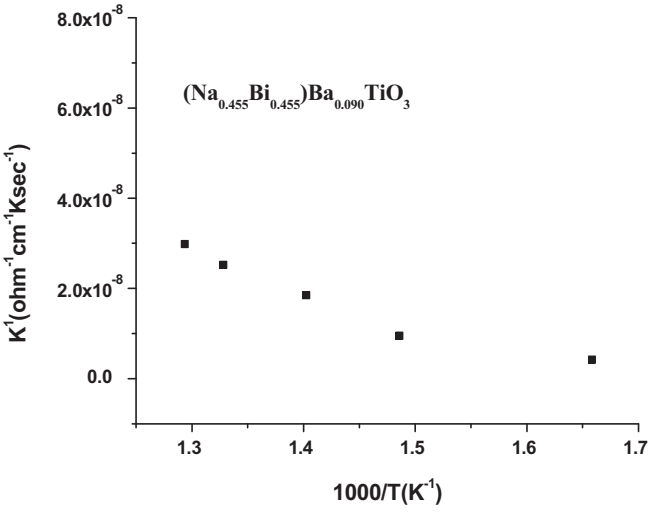

Fig. 16. Temperature dependence of charge carrier term (K^1) for BNBT90.

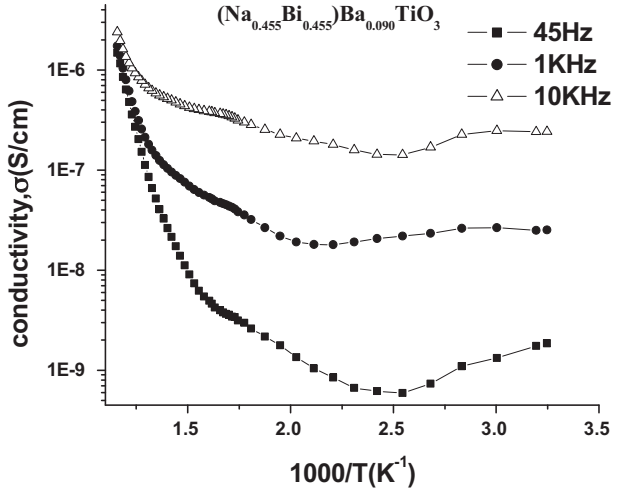

Fig. 17. Variation of conductivity as a function of inverse of temperature.

Table 4
DC and AC conductivity activation energies of BNBT90.

Temperature (°C)	Conductivity activation energy (eV) AC		
	DC	1 kHz	10 kHz
590–500	0.26	0.47	0.20
300–250	0.01	0.08	0.04
140–60	0.05	0.02	0.04

value of room temperature conductivity is 2.5×10^{-9} (S/cm) and is increased to 1.74×10^{-6} (S/cm) at 595 °C. Hence, the conductivity is observed to be increased with increase of temperature suggesting the NTCR behaviour like semiconductors. The non-appreciable variation of AC conductivity with temperature indicates the existence of multiple relaxation in BNBT90.

Further, at low temperatures, the magnitude of conductivity varies by about four orders in the frequency range under study and this behaviour changes with increasing temperature. As the temperature increases, the magnitude of conductivity is close to each other at all frequencies, curves appear to be merged at high temperatures indicating predominance of an onset of intrinsic conductivity mechanism. The activation energy for AC and DC conductivities in different temperature regions has been obtained from the Arrhenius plots (Fig. 17). The activation energies of AC and DC conductivity in the material have been evaluated and are given in Table 4.

The activation energy values for DC conductivity are found to be less than the AC conductivity. This may be due to hopping of charge carriers in the considered temperature region. Further, the AC conductivity activation energies are decreased with increase in temperature. The values of activation energies suggesting the conduction process is thermally activated and is controlled by defect-ion complexes and migration of charge species under the applied electric field. Further, the polarization field, grain boundaries may assist the charge species to migration and contributing for conductivity. The sodium ions are most mobile ions and generate the A-site vacancies. It is suggested that the sodium ion vacancies may combined with bismuth ion vacancies which undergoes from 3+ state to 4+ state or vice versa [3]. The samples are sintered at high temperature there is a chance for creation of oxygen ion vacancies. The values of activation energies reveal that oxygen vacancy migration may not be actively involved in the conduction mechanism in BNBT90.

4. Conclusions

The polycrystalline material $(Na_{0.5}Bi_{0.5})_{0.91}Ba_{0.090}TiO_3$ was prepared by conventional solid state reaction method and confirmed as tetragonal structure from XRD pattern. Dielectric studies showed a diffusive phase transition with frequency dependent dielectric maximum and relates to cation disorder at A-site, exhibits relaxor behaviour. The dielectric relaxation was modeled using Vogel–Fulcher relationship. Impedance studies reveal a non-Debye type of dielectric relaxation. Electrical modulus behaviour in the material indicating a time scale of the transition from long range mobility and are identified as the characteristics relaxation time. The conductivity parameters such as ion hopping rate (ω_p) and the charge carrier concentration (K^1) were calculated using Almond and West formalism. The increase in conductivity with increase in temperature was attributed to the increase in hopping rate with temperature. The charge carrier concentration remained almost constant over the entire temperature range, which in turn reveals that there was no creation of charge carriers over this temperature range.

Acknowledgment

Authors K.S. Rao and K.Ch. Varada Rajulu wish to thank Naval Science and Technology Laboratory (NSTL), Govt of India for the sanction of research project and Research Assistant Fellow ship.

References

[1] G.A. Smolenskii, V.A. Isupov, A.I. Agranovskaya, N.N. Krainik, Sov. Phys. Solid State 2 (11) (1961) 2651.
[2] J. Suchanicz, Ferroelectrics 209 (1998) 561.
[3] B.V. Bahuguna Saradi, K. Srinivas, G. Prasad, S.V. Suryanaryana, T. Bhimasankaram, J. Mater Sci. Eng. B 98 (2003) 10.
[4] C.S. Tu, I.G. Siny, V.H. Schmidt, Phys. Rev. B 49 (1994) 11550.
[5] J. Suchanicz, J. Kwapulinski, Ferroelectrics 165 (1995) 249.
[6] W.-C. Lee, H.H.U. Huang, L. KuoTsao, Y.-C. Wu, J. Eur. Ceram. Soc. 29 (2009) 1443.
[7] T. Takanaka, K. Maruyama, K. Sakat, Jpn. J. Appl. Phys. 30 (1999) 2236.
[8] L. Gao, Y. Huang, Y. Hu, H. Du, Ceram. Int. 33 (2007) 1041.
[9] J.R. Jurado, M.T. Colomer, J.R. Frade, J. Am. Ceram. Soc. 83 (2000) 2715–2720.
[10] J.E. Bauerle, J. Phys. Chem. Solids 30 (1969) 2657–2670.
[11] N. Hirose, A.R. West, J. Am. Ceram. Soc. 79 (1996) 1633–1641.
[12] N. Vittayakorn, G. Rujijanagul, T. Tunkasairi, X. Tan, D.P. Cann, Mater. Sci. Eng. B 108 (2004) 258.
[13] G.K. Williamson, W.H. Hall, Acta Metall. 1 (1953) 22.
[14] N. Vittayakorn, G. Rujijanagul, T. Tunkasairi, J. Mater. Res. 18 (2003) 12.
[15] K. Uchino, S. Nomura, Ferroelectrics Lett. 44 (1982) 55.
[16] S.M. Pilgrim, A.E. Sutherland, S.R. Winzer, J. Am. Ceram. Soc. 73 (1990) 3122.
[17] K. Prasad, Indian J. Eng. Mater. Sci. 7 (2000) 446.
[18] H. Vogel, Z. Phys. 22 (1921) 645.
[19] G. Fulcher, J. Am. Ceram. Soc. 8 (1925) 339.
[20] C.K. Suman, K. Prasad, R.N.P. Choudary, Adv. Appl. Ceram. 104 (2005) 294.
[21] J.R. Mac Donald (Ed.), Impedance Spectroscopy Emphasizing Solid Materials and systems, Wiley, New York, 1987.
[22] K. Prasad, K. Lily, K.P. Kumari, K.L. Chandra, S. Yadav, J. Appl. Phys. A 88 (2007) 377.
[23] N. Horose, A.R. West, J. Am. Ceram. Soc. 79 (1996) 1633.
[24] R.L. Nagai, C. Leon, Solid State Ionics 125 (1999) 81.
[25] P. Pisssis, A. Kyritsis, Solid State Ionics 97 (1997) 105.
[26] V.V. Shilov, V.V. Shevchenko, P. Pissis, A. Kyritsis, G. Georgeoussis, Y. Gommza, S.D. Nesin, N.S. Klimenko, J. Non-cryst. Solids 375 (2000) 116.
[27] D.L. Sidebottom, P.F. Green, R.K. Brow, J. Non-cryst. Solids 183 (1995) 151.
[28] J.S. Kim, T.K. Song, J. Phys. Soc. Jpn. 70 (2001) 3419.
[29] D.P. Almond, R. West, Solid State Ionics 9/10 (1983) 277.
[30] D.P. Almond, G.K. Duncan, A.R. west, J. Non-cryst. Solids 74 (1985) 285.